Analysis of the impact of surface layer properties on evaporation from porous systems using column experiments and modified definition of characteristic length

Shmuel Assouline[1], Kfir Narkis[1], Rivka Gherabli[1], Philippe Lefort[2], and Marc Prat[2]

[1]Institute of Soil, Water and Environmental Sciences, Agricultural Research Organization, Bet Dagan, Israel, [2]INPT, UPS, IMFT, Université de Toulouse, CNRS, Toulouse, France

Key Points:
- Hydraulic properties of the soil surface affect evaporation
- Methods for determining the characteristic lengths of the systems are presented
- Comparison with solution of Richards equation is presented

Correspondence to:
S. Assouline,
vwshmuel@agri.gov.il

Abstract The hydraulic properties of the layer at the vicinity of the soil surface have significant impact on evaporation and could be harnessed to reduce water losses. The effect of the properties of the upper layer on the evolution of phase distribution during the evaporation process is first illustrated from three-dimensional pore network simulations. This effect is then studied from experiments carried out on soil columns under laboratory conditions. Comparisons between homogeneous columns packed with coarse (sand) and fine (sandy loam) materials and heterogeneous columns packed with layers of fine overlying coarse material and coarse overlying fine material of different thicknesses are performed to assess the impact of upper layer properties on evaporation. Experiments are analyzed using the classical approach based on the numerical solution of Richards equation and semianalytical theoretical predictions. The theoretical analysis is based on the clear distinction between two drying regimes, namely, the capillary regime and the gravity-capillary regime, which are the prevailing regimes in our experiments. Simple relationships enabling to estimate the duration of stage 1 evaporation (*S*1) for both regimes are proposed. In particular, this led to defining the characteristic length for the gravity-capillary regime from the consideration of viscous effects at low water content differently from available expressions. The duration of *S*1, during which most of the water losses occur, for both the homogeneous and two-layer columns is presented and discussed. Finally, the impact of liquid films and its consequences on the soil hydraulic conductivity function are briefly discussed.

1. Introduction

Globally, evaporation is the main process for water vapor exchange between earth surface and atmosphere and a significant cause for water losses from natural land and irrigated fields. Evaporation from bare soils is affected by both atmospheric demand and porous-medium pore space and transport properties [*Brutsaert*, 2005]. Consequently, complex and highly dynamic interactions between medium properties, transport processes, and boundary conditions result in a wide range of evaporation behaviors as discussed by *van Brakel* [1980] and *Prat* [2002] and expressed in different suggested models [*Whitaker*, 1998; *Scherer*, 1990].

Two main stages are identified in the evaporation process: stage 1 (*S*1) with high evaporation rates mostly controlled by atmospheric conditions and stage 2 (*S*2) with low evaporation rates mostly limited by hydraulic properties of the drying porous material [*van Brakel*, 1980; *Scherer*, 1990; *Lehmann et al*., 2008]. The evaporation rate during *S*1 is often reported as constant, but this is not necessarily always the case, and maintaining a constant rate depends on the thickness of the boundary layer that develops at the soil surface [*Shahraeeni et al*., 2012]. *S*1 evaporation can be sustained as long as the drying front remains hydraulically connected to the soil surface and the phase change between liquid water to vapor occurs at the soil surface [*Scherer*, 1990; *Laurindo and Prat*, 1998; *Yiotis et al*., 2006; *Lehmann et al*., 2008]. Once the hydraulic connection to the soil surface is lost, a transition toward the *S*2 stage begins. The regime during *S*2 is characterized by the development of a dry zone adjacent to the surface of the porous medium [*Yamanaka and Yonetani*, 1999; *Saravanapavan and Salvucci*, 2000; *Assouline et al*., 2013]. Because of the poor efficiency of the transport of the water vapor by diffusion across the dry zone, the evaporation rate drops dramatically in this regime [*Salvucci*, 1997; *Shokri et al*., 2009]. Adopting this conceptual description of the evaporation process, it is evident that analytical and numerical solutions based on flow equations only, like Richards equation, cannot be applied beyond *S*1 [*Assouline et al*., 2013].

At the end of *S*1, an evaporation front (or vaporization plane) develops below the soil surface, and further drying results from vapor diffusion from that vaporization plane through the dry layer up to the soil surface [*Bristow and Horton*, 1996; *Saravanapavan and Salvucci*, 2000]. Fick's law is generally applied to estimate the diffusive evaporation rate e_{S2} based on the volumetric air content in the dry layer above the vaporization plane, the soil porosity, the vapor diffusion coefficient in free air, and the water vapor density gradient across the dry soil layer at the surface [*Moldrup et al*., 2000; *Haghighi et al*., 2013; *Or et al*., 2013]. Assuming that moisture profiles approximately preserve similarity during simultaneous drying and draining, *Salvucci* [1997] presented a time compression approximation to relate *S*1 to *S*2. This approach resulted in simple expressions for the limits of e_{S2} that depend only on the average *S*1 evaporation rate and the time between wetting and the onset of *S*2 drying.

Recent analysis of the evaporation process identified the forces controlling the extent of the hydraulically connected region during the evaporation process. These forces are the gravity, capillary, and viscous forces. The consideration of the balance between these forces led to the definition of a characteristic length *L* for the maximum extension of the hydraulically connected region, also defined as the two-phase zone, between the drying front and the soil surface [*Lehmann et al*., 2008]. That characteristic length was found to depend on the pore size range between the smallest and largest pores, which can be deduced from the water retention curve, a key hydraulic function of porous media. As a result, cumulative water losses and depth of the drying front at the end of *S*1 are strongly related to *L*. Equivalent computations were carried out by *Prat and Bouleux* [1999] for the special case of 2-D porous media, which implies considering the particular structure of the two-phase zone near a percolation threshold. This led to a nontrivial scaling of *L* with the dimensionless numbers characterizing the pore size distribution and the balance between the forces at play. More details on the difference between the 2-D and 3-D cases can be found in *Prat et al*. [2012, and references therein].

Introducing media-related characteristic lengths can also be useful for addressing the issue of the effect of heterogeneity in the porous media properties on evaporation [*Lehmann and Or*, 2009; *Shokri et al*., 2010]. Considering evaporation from layered sand columns, *Shokri et al*. [2010] proposed a composite characteristic length that accounts for sand properties and layer thicknesses and positions. They showed that air invading an interface between fine and coarse sand layers results in a capillary pressure jump that affects liquid phase distribution compared to the homogeneous case.

Although many of the works cited above were based on traditional continuum concepts, the understanding and analysis of evaporation process can be also performed, thanks to pore network (PN) modeling and invasion percolation theory [*Prat*, 1993; *Laurindo and Prat*, 1998; *Prat and Bouleux*, 1999; *Huinink et al*., 2002; *Plourde and Prat*, 2003; *Prat*, 2007; *Chapuis and Prat*, 2007; *Chraibi et al*., 2009]. This notably permits to study situations that cannot be analyzed properly with the traditional continuum approach, such as the 2-D situation mentioned previously or, for example, the formation of efflorescence discrete spots at the evaporative surface of a porous medium [*Veran-Tissoires et al*., 2012]. The PN approach is also well adapted for modeling explicitly the impact of capillary liquid films on evaporation [*Yiotis et al*., 2003, 2012; *Prat*, 2007]. The impact of those liquid films on evaporation process can be huge [*Chauvet et al*., 2009], depending on the microgeometry of porous medium, pore size, and the evaporative conditions. The PN approach and associated theories are also well adapted to the study of heterogeneous media. First insights on evaporation in a two-layer system were obtained combining PN simulations and experiments with an etched network for a two-layer porous medium [*Pillai et al*., 2009]. In particular, this study indicated significant difference in drying rate and fluid invasion pattern depending on which of the two layers, coarse or fine, was in contact with the external air.

Evaporation is a process occurring at the interface between the bare soil and the atmosphere. Therefore, a key element that determines evaporation dynamics is the physical properties of the upper layer at the vicinity of the soil surface. These properties can be significantly altered by different natural processes or following anthropogenic interventions, thus affecting fluid fluxes through that surface. An example of a natural process is the formation of a seal layer at the surface of a bare soil exposed to the impacts of raindrops during high-kinetic energy rainfall [*Assouline*, 2004]. The hydraulic properties of this more compacted and less permeable layer at the soil surface reduce infiltration [*Assouline and Mualem*, 1997; *Assouline et al*., 2007] but also evaporation rates [*Bresler and Kemper*, 1970; *Assouline and Mualem*, 2003]. In agricultural systems, tillage and mechanical compaction are common practices, tillage creating a loose upper layer in the soil profile

while mechanical compaction causing the opposite. The corresponding changes in the hydraulic properties of the cultivated upper soil layer [*Assouline*, 2006a, 2006b] will necessarily affect the corresponding characteristic lengths and the related flow processes. Less water was found to evaporate from tilled soils compared to untilled ones [*Holmes et al*., 1960; *Moroizumi and Horino*, 2002]. This is in agreement with the well-established result that a coarse-textured layer overlying fine-textured soil suppresses evaporation [*Willis*, 1960; *Diaz et al*., 2005]. This result led to the application of mulch layers of coarse material on the soil surface to reduce water losses from evaporation [*Unger*, 1971; *Modaihsh et al*., 1985; *Mellouli et al*., 2000; *Yamanaka et al*., 2004].

The presence of the coarse upper layer at the surface accelerates the loss of hydraulic connectivity from the drying front to the soil surface and, consequently, reduces the duration of *S*1 and induces a rapid transition to the *S*2 regime characterized by much lower evaporation rates. Therefore, the fact that the coarse-over-fine (or loose-over-compacted) configuration at the soil surface reduces evaporative water losses is widely accepted.

This is not the case when the fine-over-coarse configuration at the soil surface is considered. The experimental results of *Bresler and Kemper* [1970] regarding the reduced evaporation from a soil column with a seal layer at the surface compared to a homogeneous one are in apparent contradiction with the findings of *Willis* [1960] that reported that little difference on evaporation rate was observed from a system of fine overlying coarse-textured soil compared with homogeneous fine-textured soil. Two elements differed in the respective experimental setups that could contribute to explain the apparent contradiction: (a) thickness of the overlying layer (up to few centimeters for the seal layer versus 30 cm for the fine-textured soil layer) and (b) initial condition (evaporation measured immediately after wetting for the sealed column versus evaporation from a water table 80 cm below surface in the layered columns) that induced differences in the evaporation rate (1.8 cm/d in the sealed column versus 0.3 cm/d in the fine overlying coarse-textured configuration in the layered columns).

We thus propose to investigate in more depth the impact of soil surface properties on evaporation in general, and the effect of the thickness of the overlying layer in particular. The applied methodology relies on a combination of theoretical analysis and modeling based on the continuum approach, few pore network simulations providing illustrative phase distributions and experimental data from laboratory scale experiments on homogeneous and heterogeneous vertical soil columns.

To a certain extent, the present work can be seen as a continuation of the work presented in *Shokri et al*. [2010]. The main differences lie in a modified definition of characteristic length and a clear distinction between two drying regimes, namely, the capillary regime and the gravity-capillary regime. This distinction was not explicit in *Shokri et al*. [2010]. Also, *Shokri et al*. [2010] focused on the prediction of the front depth (size of two-phase zone at the end of *S*1). By contrast, the emphasis in the present paper is on the use of characteristic length for predicting the mass loss, i.e., the duration of *S*1.

2. Pore Network (PN) Simulations

Some numerical simulations of the process of evaporation from two-layer porous systems based on three-dimensional pore networks are presented first to illustrate some of the concepts used in the following sections. Pore network (PN) models of drying can now be considered as a classical tool for the study of drying problems [*Prat*, 2002, 2011]. The simpler model of this type [*Prat*, 1993] can be regarded as a variant of the classical invasion percolation (IP) algorithm presented by *Wilkinson and Willemsen* [1983], which introduces a dynamic aspect via the computation of evaporation from the various liquid clusters that form during the evaporation process. From the experiments reported in *Laurindo and Prat* [1996] and the PN simulations reported in *Le Bray and Prat* [1999], it is also well established that the evolution of phase distribution during *S*1 can be simulated using PN models. As discussed for example in *Laurindo and Prat* [1996], it is fairly easy to take into account the gravity effects in addition to capillary effects in this type of model. Since here the PN simulations are simply used for illustrating some aspects of the phase distribution during the evaporation process in layered systems, the PN algorithms will not be presented. The interested reader can refer to the aforementioned references for the details. Note that the liquid film effect is not considered in the PN simulations presented in what follows.

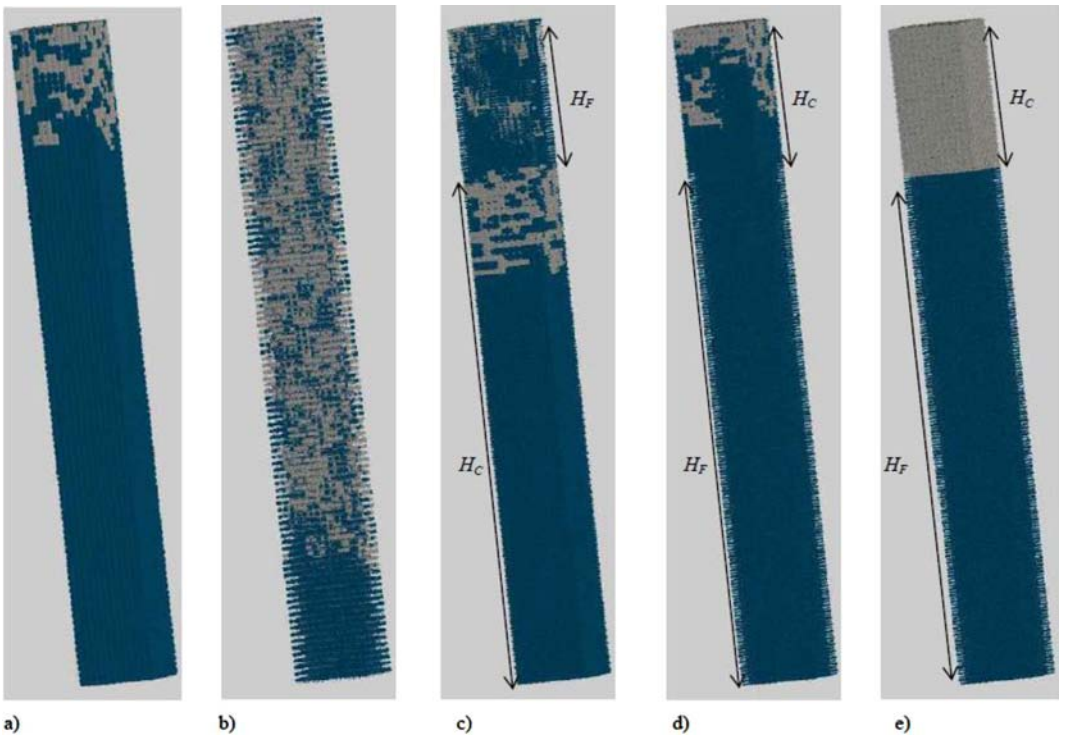

Figure 1. Examples of phase distribution in a column of square cross section and of total height H obtained using pore network simulations (the liquid phase is in blue, the gas phase in gray): (a) coarse porous medium at the end of $S1$; (b) fine porous medium at the end of $S1$; (c) fine layer (thickness H_F) over coarse medium when the liquid phase in the coarse region ceases to be hydraulically connected to the top fine layer; (d) coarse layer (thickness H_C) over fine medium at the end of $S1$; (e) coarse layer over fine medium when the coarse layer is entirely dry and the fine layer begins to dry. Evaporation (gas invasion) is from top surface only. The size of network is $16 \times 16 \times 100$. The thickness of the top layer in Figures 1(c)–1(e) is 24.

2.1. Network Design

The PN simulations were carried out using a ($16 \times 16 \times 100$) cubic network. Using the distance between two pores (the lattice spacing) as unit length, the width of the column is $l = 16$, and its height length is $H = 100$. In the cases of two-layer systems, the thickness of the overlying coarse or fine layer, H_C or H_F, respectively, is 24. The size of the throats in the fine porous medium was randomly distributed according to a uniform probability density function in the range [0.15, 0.26] with a mean value $\bar{d} = 0.21$, and in the coarse porous medium in the range [0.70, 0.80] with a mean value $\bar{d} = 0.75$. Gravity forces are specified so as to obtain a short characteristic length in the coarse medium and a long one in the fine medium, in qualitative similarity with the column experiments presented below.

2.2. Phase Distributions in Homogeneous and Layered Networks

Some phase distributions of interest obtained, thanks to 3-D pore network simulations, are depicted in Figures 1a–1e. Figure 1a shows the maximum extent of the two-phase zone (=end of $S1$) obtained with the coarse pore network whereas Figure 1b shows a similar picture for the fine pore network. Note that trapped liquid clusters are not considered in the discussion. The salient feature is that the extent of the two-phase zone when the surface ceases to be hydraulically connected to the liquid still present in the network is much greater in the fine network. This is of course a direct consequence of the competition between gravity and capillary effects.

Figure 1c shows what happens when a relatively thin layer of fine medium, i.e., much thinner than the characteristic length of the fine medium, is on top of a much thicker coarse layer. As discussed in many previous works, slow drying is essentially an invasion percolation process. Since the capillary pressure threshold (CPT) of a constriction in the pore space (CPT = pressure difference across a meniscus stuck in a constriction that must be overcome for displacing the meniscus) is inversely proportional to the characteristic size of the constriction, the CPTs in the fine porous medium are greater than in the coarse porous medium. The result is the preferential invasion of the coarse porous medium as soon as the gas phase has crossed the

fine porous layer [*Pillai et al*., 2009]. Note that the capillary pressure is relaxed and may initiate fast fluid redistribution when air enters the coarse material [see *Shokri et al*., 2010]. This phenomenon is not accounted for in the present simulations. Then the invasion continues into the coarse porous medium until the two-phase zone that forms into this medium ceases to be hydraulically connected to the interface between the fine and the coarse media. This is the particular moment which is shown in Figure 1c. From that moment, drying continues into the fine porous medium until the lost of the hydraulic connection of the top surface with the rest of the system marking the end of phase *S*1.

Figures 1d and 1e show fluid distributions corresponding to the case where the upper thinner layer is coarse and the underlying thicker layer is fine. Here we have considered that the characteristic length of the coarse porous medium was smaller than its thickness. As a result, the end of stage *S*1 is expected to occur exactly as for an entirely coarse porous medium, namely, when the extent of the two-phase zone in the coarse top layer reaches the characteristic length of the coarse porous medium. This is the situation illustrated in Figure 1d. Then, since it is easier to displace the menisci in the coarse layer, the full drying of the upper coarse layer is expected to occur before gas invasion takes place in the fine porous layer. This is the situation illustrated in Figure 1e.

The phenomenology illustrated in Figures 1a–1e will be useful to discuss the modeling of the *S*1 regime based on the continuum approach presented in section 3.

3. Theory and Modeling Based on the Continuum Approach

3.1. Main Drying Regimes

As emphasized above, the prediction of duration of *S*1 is a key issue in the analysis of evaporation process. The basic idea is that *S*1 ends when the maximal size of the two-phase zone is reached. Then, the two-phase zone travels deeper within the sample, and a growing dry zone forms adjacent to the porous medium surface. This obviously holds only when the maximum extent of the two-phase zone is shorter than the height of sample. As discussed in *Prat* [2002], three main regimes can be in fact distinguished with regards to the evolution of the two-phase zone. In the capillary regime, the extent of the two-phase zone is limited by the height *H* of sample, i.e., the two-phase zone can span the sample. This is the situation observed when gravity and viscous effects are negligible compared to capillary forces. In the gravity-capillary (or viscosity-capillary, respectively) regime, the two-phase zone is confined, i.e., shorter than the sample height, as a result of the competition between gravity (or viscous forces, respectively) and capillary forces. It is important to realize that only the gravity-capillary and viscous-capillary regimes were considered in previous works, e.g., *Lehmann et al*. [2008], with regards to the determination of the duration of *S*1 in relation with the so-called characteristic length.

For analyzing the evaporation from layered systems considered in the present study, the capillary regime must also be considered (as it will be made clear later, this corresponds to the situation where a coarse layer shorter than its gravity-capillary or viscous-capillary characteristic length is on top of a finer medium, for example). In the present paper, we thus propose also a simple expression for estimating the duration of *S*1 in the capillary regime. The proposed expression is tested against experimental data.

It should be noted that the porous media in our experiments are relatively coarse. As a result, we are only interested in the capillary and the gravity-capillary regimes.

3.2. Homogeneous Profiles (Gravity-Capillary Regime)

The gravity-capillary regime is the simplest regime for estimating the characteristic length of the two-phase zone, at least for a homogeneous medium [*Lehmann et al*., 2008]. For convenience, the expression of the characteristic length proposed by *Lehmann et al*. [2008] is recalled and can be expressed as

$$L = \frac{1}{\alpha(n-1)} \left(\frac{2n-1}{n}\right)^{(2n-1)/n} \left(\frac{n-1}{n}\right)^{(1-n)/n} \tag{1}$$

where the various parameters come from the representation of the water retention curve of the porous medium using the van Genuchten model [*van Genuchten*, 1980]

$$\Theta = \frac{\theta - \theta_r}{\theta_s - \theta_r} = \left[\frac{1}{1+(\alpha h)^n}\right]^m \tag{2}$$

where Θ is the effective saturation, $\theta(h)$ the volumetric water content, h the pressure head, θ_r the residual water content, θ_s the water content at saturation (=porosity), α the inverse of a characteristic pressure head, n a fitting parameter, and $m = 1 - 1/n$.

It should be pointed out that the thickness of the two-phase zone considered in *Lehmann et al*. [2008] corresponds to the distance from the soil surface to the drying front and does not include the capillary fringe since the pores were supposed to be completely filled by water in the capillary fringe (in line with the *Brooks and Corey* [1964] model for the water retention curve). The height of the capillary fringe corresponds to the air-entry pressure h_b, which can be evaluated according to *Lehmann et al*. [2008] as

$$h_b = \frac{1}{\alpha}\left(\frac{n-1}{n}\right)^{(1-2n)/n} - L \tag{3}$$

In fact both h_b and L were determined from an approximation consisting in linearizing the retention curve, which was expressed, for h given in absolute values and $|h| \geq |h_b|$ as

$$\theta = \frac{\theta_s - \theta_t}{h_b - h_t}(h - h_b) + \theta_s \tag{4}$$

where h_t and θ_t are the pressure and water content at the inflexion point of the retention curve (see *Lehmann et al*. [2008] for more details).

In what follows, we propose a slightly different way of determining the thickness of the two-phase zone starting from a classical model of liquid flow, i.e., the Richards equation, which is valid to describe the evolution of the saturation profile during *S*1. Since the evaporation flux is known during *S*1, the remaining main characteristic of interest is the phase distribution that is the saturation profile. The total mass of liquid loss is simply given by the mass balance

$$\frac{dM}{dt} = -Aj \tag{5}$$

where M is the mass of liquid in the column, A is the area of the evaporative surface, and j is the evaporation flux expressed in [M/L^{-2}/T^{-1}]. Assuming that j is approximately constant during *S*1 and close to the potential evaporation, j_0, $j \approx j_0$, equation (5) becomes

$$M = M_0 - A\ j_0\ t \tag{6}$$

where M_0 is the initial mass of liquid in the domain, with $M_0 = \rho_l A\ \theta_s H$, H being the height of the soil column and ρ_l the liquid density. The mass M can be also expressed from the water content profile $\theta(z)$

$$M = \rho_\ell A \int_0^H \theta(z)dz \tag{7}$$

where θ is the water content and z is a vertical coordinate starting from the top surface of column and directed downward. Combining equations (6) and (7) yields

$$\theta_s H - e_0 t = \int_0^H \theta(z)dz \tag{8}$$

where $e_0 = \frac{j_0}{\rho_\ell}$ is the potential evaporation expressed in [L T^{-1}]. Denoting by $H_s(t)$ the thickness of the two-phase zone in the column, equation (8) can be expressed as

$$e_0 t = \int_0^{H_s(t)} (\theta_s - \theta(z))dz \tag{9}$$

where $H_s(t)$ and θ(z) are the two unknowns of the problem.

During *S*1, the saturation profile is governed by the classical flow equations describing one-dimensional flow in the two-phase region

$$\frac{\partial \theta}{\partial z} + \frac{\partial q_z}{\partial z} = 0 \tag{10}$$

with

$$q_z = K(\theta)\left(\frac{\partial h}{\partial z} + 1\right) \tag{11}$$

where $K(\theta)$ the hydraulic conductivity and q_z the flux in the z direction. At the evaporative surface, we express the continuity of the flux by

$$q_z = K(\theta)\left(\frac{\partial h}{\partial z} + 1\right) = -e_0 \tag{12}$$

Suppose now that the phase distribution is very close to a hydrostatic distribution, as shown by *Shimojima et al*. [1990]. This distribution is simply given by

$$\frac{\partial h}{\partial z} = -1 \tag{13}$$

which leads to

$$h(\theta) = H_s(t) - z \tag{14}$$

Using the van Genuchten representation for the water retention curve (equation (2)) yields

$$\frac{\theta - \theta_r}{\theta_s - \theta_r} = \left[\frac{1}{1 + (\alpha(H_s(t) - z))^n}\right]^m \tag{15}$$

which is combined with equation (8) to obtain

$$(\theta_S - \theta_r) \int_0^{H_s(t)} \left(1 - \left[\frac{1}{1 + (\alpha(H_s(t) - z))^n}\right]^m\right) dz = e_0 t \tag{16}$$

This equation can be solved numerically to determine the evolution of the position of the maximum extent of the two-phase zone during *S*1, $H_s(t)$. However, equation (16) does not provide any information on the maximum extent of the two-phase zone at the end of *S*1, H_{smax}. In other words, equation (16) can be used only as long as

$$H_s(t) \leq H_{\text{smax}} \tag{17}$$

To determine the duration of *S*1 from equation (16) and other related characteristics of interest such as the cumulative evaporation during *S*1 or the water content profile at the end of *S*1, etc., it is therefore crucial to

estimate H_{smax} independently. As mentioned before, and in accordance with *Shokri and Salvucci* [2011], H_{smax} is expressed as

$$H_{smax} = L + h_b = \frac{1}{\alpha}\left(\frac{n-1}{n}\right)^{(1-2n)/n} \tag{18}$$

where h_b and L are given by equations (1) and (3).

Lehmann et al. [2008] provides a simplified approach to estimate the characteristic length of the two-phase zone, which can be also used together with equation (16) to predict the duration of *S*1. It can be noted that a further simplification was proposed by *Lehmann et al.* [2008] with regard to the cumulative mass of water evaporated at the end of S_1, M_{S1}. From the suggested linearization of the retention curve (equation (4)), this mass was expressed as $M_{S1} = \frac{1}{2}(\theta_s - \theta_r)\rho_\ell AL$, or in terms of evaporation depth (equivalent thickness of liquid water), by

$$E_t = \frac{1}{2}(\theta_s - \theta_r)L \tag{19}$$

With all these simplifications, the duration of S_1 is then simply given by

$$t_{S1} = \frac{E_t}{e_0} = \frac{1}{2}\frac{(\theta_s - \theta_r)L}{e_0} \tag{20}$$

This gives a very simple way of estimating the duration of *S*1 as well as the extent of the two-phase zone at the end of *S*1. The comparisons with experimental date reported in *Lehmann et al.* [2008] led to a reasonable agreement with regard to the two-phase zone extent (front depth) but the measured mass loss at the end of *S*1, i.e., the measured duration of *S*1, was higher than predicted. This suggests that the definition of characteristic length can be improved so as to obtain better predictions of the duration of *S*1. An attempt is made in this direction in what follows, from a slightly more detailed analysis of what happens at the end of *S*1. Equations (19) and (20) assume that the water content marking the end of *S*1, θ_v, is equal to the residual water content θ_r. From physical ground, it is in fact expected that θ_v depends on the evaporation rate because the viscous effects become necessarily nonnegligible when the water content approaches θ_v (or θ_r). The picture is to consider that the phase distribution is essentially controlled by the capillary-gravity equilibrium over most the saturation profile but depends on viscous effects only in the region of low water content. In this (small) region, we express the continuity between the evaporation flux and liquid flow according to equation (12) where we consistently neglect the gravity term since viscous effects becomes dominant

$$K(\theta_v)\frac{\partial h}{\partial z} = -e_0 \tag{21}$$

which provides the possibility to determine θ_v characterizing the end of S_1. A similar approach was already proposed by *Coussot* [2000] in his analysis of the simpler situation where the water content was assumed uniform. The viscous effects become comparable to the gravity effects when the pressure variation in the liquid is comparable to the hydrostatic variation, namely, when $\frac{\partial h}{\partial z} \approx -1$ in equation (21). This leads to

$$K(\theta_v) = e_0 \tag{22}$$

where θ_v is thus the cross-over water content for which the gravity and viscous effects lead to a pressure drop of comparable magnitudes in the liquid. Note that θ_v consistently tends toward θ_r as the evaporation flux decreases. Using the Mualem model for the hydraulic conductivity function [*Mualem*, 1976], equation (22) can be expressed as

$$K_s \Theta_v^{0.5}\left[1 - \left(1 - \Theta_v^{1/(1-1/n)}\right)^{1-1/n}\right]^2 = e_0 \tag{23}$$

where $\Theta_v = \frac{\theta_v - \theta_r}{\theta_s - \theta_r}$ and K_s is the hydraulic conductivity of the considered porous medium. Once Θ_v is determined from equation (23), one can determine the corresponding pressure head from van Genuchten's relationship (equation (2))

$$h_v = \frac{1}{\alpha}\left(\frac{1}{\Theta_v{}^{1/m}} - 1\right)^{1/n} \tag{24}$$

leading to the following estimate for H_{smax}:

$$H_{\mathrm{smax}} = h_v = \frac{1}{\alpha}\left(\frac{1}{\Theta_v{}^{1/m}} - 1\right)^{1/n} \tag{25}$$

If, as in *Lehmann et al*. [2008], the capillary fringe is not included in the estimate of the two-phase zone thickness, this gives the following estimate of the new characteristic length L^*:

$$L^* = H_{smax} - h_b \tag{26}$$

where H_{smax} and h_b are given by equations (24) and (3), respectively.

3.3. Homogeneous Profiles (Capillary Regime)

In the capillary regime, gravity forces can be neglected and, as mentioned before, the two-phase zone becomes as wide as the sample height. Furthermore, this regime is characterized by spatially uniform water content [*Le Bray and Prat*, 1999]. Since the water content is uniform and the only (macroscopic) length scale is the sample height H, we propose to estimate the duration of $S1$ in the capillary regime from the expression

$$K(\theta_v)\frac{\partial h}{\partial z} \approx K(\theta_v)\frac{h(\theta_v)}{H} = e_0 \tag{27}$$

where θ_v is the water content marking the end of $S1$. Equation (27) is solved to determine θ_v. This finally leads to the following estimate for the duration of $S1$ is the capillary regime:

$$t_{S1} = H\frac{(\theta_s - \theta_v)}{e_0} \tag{28}$$

It can, in fact, be expected than $\theta_v \approx \theta_r$. Thus,

$$t_{S1} \approx H\frac{(\theta_s - \theta_r)}{e_0} \tag{29}$$

which indicates that the duration of $S1$ can be expected to be linearly proportional to the height of sample in the capillary regime.

Physically, equation (27) expresses in fact that viscous effects eventually limit the duration of $S1$ in the capillary regime since the hydraulic conductance of liquid phase significantly decreases at low water contents.

3.4. Two-Layer Profiles: Fine Over Coarse Material Case (F/C)

In the case of a layer of fine material overlying a coarse porous medium, we will assume that the thickness H_F of the fine layer is much smaller than the characteristic length of the homogeneous fine medium, hence $H_F << L_F$. The phenomenology is as follows in this case: the gas phase invades the fine layer and rapidly reaches the coarse layer. The water content in the fine layer when the coarse layer is reached is close to the water content corresponding to the fine porous medium gas entry pressure (percolation threshold of the fine porous medium), hence $\theta_F \approx \theta_{s-F}$, θ_{s-F} being the saturated water content of the fine material. Then gas invasion takes place in the coarse porous layer, which is characterized by lower pore space constriction capillary pressure thresholds until the invasion depth in the coarse layer reaches the characteristic length L_C of the coarse porous medium. The mean position of the most advanced points of the invasion front is therefore at a depth $(H_F + L_C)$ from the surface when this time is reached. This time corresponds to the moment where the coarse porous medium ceases to be hydraulically connected to the fine porous medium. As a

result, a second phase begins where the fine layer resumes drying. When this happens, the evaporated mass (expressed in [LT^{-1}]) is given by

$$(\theta_{s-C}-\theta_{r-C})\int_{H_F}^{L_C+H_F}\left(1-\left[\frac{1}{1+(\alpha_C(L_C-z+H_C))^{n_C}}\right]^{m_C}\right)dz=e_0 t_{1-C} \tag{30}$$

where t_{1-C} is the duration of *S*1 for the homogeneous coarse porous medium. The values of exponents n_C and m_C in equation (30) are those corresponding to the coarse medium in equation (2).

Then the stage *S*1 continues until the water content has sufficiently decreased in the overlying fine layer. Since $H_F \ll L_F$, gravity effects can be neglected in the fine layer and the water content can be considered as uniform over the fine layer (capillary regime). Accordingly, we again express that *S*1 ends when the viscous effects become too high for maintaining the flux at the surface, that is,

$$K(\theta_{v-F})\frac{\partial h}{\partial z}=-e_0 \tag{31}$$

where after using again the approximation $\frac{\partial h}{\partial z}\approx\frac{h(\theta_{v-F})}{H_F}$ gives

$$K(\theta_{v-F})\frac{h(\theta_{v-F})}{H_F}=e_0 \tag{32}$$

which provides the possibility to estimate the water content θ_{v-F} in the fine layer that characterizes the end of S_1. The corresponding elapsed time is

$$\delta t=\frac{H_F(\theta_{s-F}-\theta_{v-F})}{e_0} \tag{33}$$

In summary, the characteristic length of the *F/C* two-layer system is

$$L_{F/C}=H_F+L_C \tag{34}$$

which is similar to the result presented in *Shokri et al.* [2010] for the (*F/C*) case with $L_F >> H_F$. The duration of *S*1 is given by

$$t_{S1}=t_{1-C}+\delta t=t_{1-C}+\frac{H_F(\theta_{s-F}-\theta_{v-F})}{e_0} \tag{35}$$

where we recall that t_{1-C} is the duration of *S*1 for the coarse medium homogeneous column (equation (30)). Therefore, the evaporation depth from the (*F/C* system), $E_{F/C}$, is given by

$$E_{F/C}\approx e_0\ t_{1-C}+H_F(\theta_{s-F}-\theta_{v-F})\approx \mathrm{E_C}+H_F(\theta_{s-F}-\theta_{v-F}) \tag{36}$$

where E_C is the evaporation depth for the homogeneous coarse porous medium. Consequently

$$\frac{E_{F/C}}{L_{F/C}}\approx\frac{E_C+H_F(\theta_{s-F}-\theta_{v-F})}{L_C+H_F} \tag{37}$$

Under the condition of very slow evaporation, one can furthermore assume that $\theta_{v-F}\approx\theta_{r-F}$, which leads, since $\theta_{r-F}<<\theta_{s-F}$, to the following expression for the evaporation depth:

$$E_{F/C} \approx e_0\ t_{1\text{-}C} + H_F\theta_{s-F} \approx \mathrm{E_C} + H_F\theta_{s-F} \tag{38}$$

and thus

$$\frac{E_{F/C}}{L_{F/C}} \approx \frac{E_C + H_F\theta_{s-F}}{L_C + H_F} \tag{39}$$

3.5. Two-Layer Profiles: Coarse Over Fine Material Case (C/F)

When the coarse layer is on top and the fine layer below, several situations may be encountered depending of the ratio between the thickness H_C of the coarse layer and the characteristic length L_C of the coarse medium. In the case where there is no overlap between the pore size distributions in the coarse material and in the fine material, the phenomenology is simple and characterized by the full drying of coarse porous medium before invasion of the underlying fine medium by the gas phase starts as a result of evaporation.

When $L_C << H_C$, the presence of the underlying fine porous medium has no influence on the duration of *S*1, which is expected to be controlled by the coarse medium only. Thus, in such case,

$$L_{C/F} = L_C \tag{40}$$

and the duration of *S*1 (or equivalently the evaporation depth) can be determined as in section 3.1.

When $L_C >> H_C$, gravity effects become negligible and the moisture content is therefore spatially uniform over the thickness of the coarse layer during *S*1 (capillary regime). Thus we can use similar arguments as in section 3.3 to determine the end of stage *S*1. We express that stage *S*1 ends when the moisture content satisfies the equation

$$K(\theta_{v-C})\frac{h(\theta_{v-C})}{H_c} = e_0 \tag{41}$$

which provides the possibility to estimate the water content $\theta_{v\text{-}C}$ in the coarse layer that characterizes the end of S_1. Naturally, the hydraulic conductivity function and water retention curve in equation (41) are those of the coarse material. The corresponding duration t_{S1} is

$$t_{S1} = \frac{H_C(\theta_{s-C} - \theta_{v-C})}{e_0} \tag{42}$$

and the characteristic length of the *C/F* two-layer system can be defined as

$$L_{C/F} \approx H_C \tag{43}$$

in this case, although it should be clear that the end of stage *S*1 does not correspond to the time when the gas phase reaches the coarse-fine interface for the first time.

The situation may be subtler in case of a nonnegligible overlap between the two pore size distributions. In such case, the result will be a partial invasion of the fine material before the end of *S*1 contrary to the situation considered in this section.

3.6. Applicability of Richards Equation

The direct applicability of Richards equation is limited to *S*1 evaporation since, during *S*2, a dry layer is formed at the soil surface in which the transport mechanism is mainly vapor flow along moisture and temperature gradients, thus invalidating the application of approaches based on liquid transport [*Philip*, 1957]. However, based on the conclusions of *Milly* [1984] regarding the relative low global impact of thermal and vapor fluxes, *Salvucci* [1997] assumed that daily averaged *S*2 evaporation rates could be considered to be limited by liquid flow from deeper soil layers so that Richards equation could still be applicable. Several studies have applied such approach, some of them using the Hydrus software [*Simunek et al*., 2005] to solve

Figure 2. Experimental setup for the homogeneous and the two-layer columns (the brown soil in the sandy loam, and the gray one is the coarse sand). The fans at the top of each column are shown.

numerically the flow equations [*Saito et al*., 2006, *Sakai et al*., 2009]. This will be tested from comparisons with our experimental results.

3.7. Computation of Characteristic Length From Richards Equation

Since the Richards equation can be used with some confidence during *S*1, it is interesting to compute the characteristic length for the gravity-capillary regime from the numerical solution to Richards equation. The obtained results can be regarded as reference results in order to assess the quality of the two analytical methods presented in section 3.1 since the determination of the characteristic length is made without approximation (if one accepts the validity of Richards equation during *S*1 of course). The procedure, explained in details in the next section, is as follows. Richards equation is solved using Hydrus-1D [*Simunek et al*., 2005] imposing as upper boundary condition the evaporation rate e_0 (Neuman-type boundary condition) until the capillary potential at the surface reaches a prescribed high absolute value above which the system cannot sustain anymore the e_0 rate and the upper boundary condition switches to a Dirichlet-type boundary condition (constant prescribed capillary potential at the surface; see Hydrus user manual for more details). From the profile $h(z)$ obtained at this particular time, which corresponds to the end of *S*1, the characteristic length is determined as the distance between the surface and the point where $h = h_b$ (we recall that h_b is the air-entry pressure of the considered medium). Naturally, the numerical computation also gives the cumulative evaporation at the end of *S*1.

4. Methodology

4.1. Laboratory Experiments

Unless otherwise mentioned, laboratory scale experiments were carried out on 50 cm height and of 8 cm in diameter Plexiglas columns packed with coarse sand (C) and a fine-textured sandy loam soil (F) to create a variety of two-layer configurations. To provide reference evaporation rates characterizing each one of the porous media used, columns were also homogeneously packed with each one of the two materials. The mean particle size of the coarse sand was 2.0 mm (1.5–2.5 mm) while that of the sandy loam was approximately 0.1 mm. Packing of the coarse sand was achieved at a bulk density of 1.57 ± 0.05 g cm^{-3} and that of the sandy loam, at a bulk density of 1.39 ± 0.03 g cm^{-3}. The following configurations of packed columns were considered: (a) homogeneous coarse sand; (b) homogeneous fine sandy loam; (c) layers of sandy loam with 2, 8, and 12 cm thickness overlying coarse sand (F/C case); layers of coarse sand with 2 and 12 cm of overlying fine material (C/F case). A picture of the setup is presented in Figure 2. After being packed under dry conditions, the columns were gently saturated from below with tap water up to the soil surface. The bottom was then sealed (lower boundary condition of zero flux) and the columns exposed to drying. It is to note that this specific lower boundary condition does not represent field conditions where drainage and drying generally occur simultaneously.

A small individual fan (Spire Corp., Netherlands), generating wind speed of approximately 1.5 m/s, was installed close to the open upper top of each column, constantly blowing wind parallel to the evaporating surface. Replicate columns were used in most cases to check the reproducibility of the results. Potential evaporation rate during the experiment was characterized by evaporation from a column filled with water and subjected to similar conditions. The columns were weighted every 15 min using electronic scales (Merav 2000, Shekel, Beit-Keshet, Israel) with an accuracy of ± 0.5 g that were connected to a data logger

Table 1. Parameters Corresponding to the Measured Hydraulic Functions of the Coarse Sand (C) and the Sandy Loam (F) and the Estimated Parameters Corresponding to the Soil Packed in the Columns Used in the Experiments and Presented in Figure 4

		θ_s (cm^{-3} cm^{-3})	θ_r (cm^{-3} cm^{-3})	α (cm^{-1})	n	h_b (cm)	K_s (cm h^{-1})
Coarse sand (C)	Measured	0.34	0.001	0.17	6.04	−4.3	253.8
	Estimated (column)	0.41	0.0009	0.25	5.84	−2.92	232.1
	Inverse (Hydrus)	0.41	0.00003	0.25	2.48		41.2
Sandy loam (F)	Measured	0.45	0.01	0.023	3.65	−22.5	36.3
	Estimated (column)	0.48	0.01	0.033	3.96	−15.4	31.2
	Inverse (Hydrus)	0.48	0.024	0.033	3.39		8.3

(CR1000, Campbell Scientific Inc., USA). Water mass loss and evaporation rate corresponding to each column were computed from the data.

The hydraulic properties, namely, the saturated hydraulic conductivity K_s and the water retention curve (WRC), of disturbed samples of the coarse and fine materials, were measured under laboratory conditions in duplicates. The samples for the measurements of K_s were packed at bulk densities of 1.55 and 1.35 g/cm^3 for the sand and the sandy loam, respectively. The samples for the measurements of the WRC were packed at bulk densities of 1.75 and 1.54 g/cm^3 for the sand and the sandy loam, respectively. The expression in equation (2) was fitted to the measured WRC. The corresponding parameters and the K_s values are presented in Table 1 (*measured* values). Since the columns of the drying experiments were packed at different bulk densities than the samples used for the direct measurements of the hydraulic properties, the hydraulic functions representing the soils packed in the columns used in the experiments were estimated following the models presented in *Assouline* [2006a, 2006b]. The corresponding values of the different parameters after the correction for the respective packing bulk densities are shown in Table 1 (*estimated* values). The results of the measured and estimated WRC for the sand and the sandy loam are depicted in Figure 3.

4.2. Numerical Simulations Based on the Solution of Richards Equation

As mentioned before, simulations were performed using Hydrus-1D [*Simunek et al.*, 2005]. To investigate the applicability of Richards equation, two approaches were applied: (a) using the estimated parameters listed in Table 1 to define the soil hydraulic functions; (b) applying an inverse approach based on the measured evaporation rates with time to determine the most appropriate parameters defining the hydraulic functions of the two soils. For the first case, the upper boundary condition was the measured mean daily constant e_0 rate from the water column, and shifted to a constant prescribed capillary potential at the surface ($h_{A-C} = 1$ bar for the coarse sand and $h_{A-F} = 10$ bar for the sandy loam) when the soil surface reached that limit and the system could not sustain anymore the e_0 rate. The upper boundary condition for the inverse procedure was provided by the measured actual daily $e(t)$ rates from the respective soil columns. A soil profile of 50 cm depth, with a space discretization of 1.0 cm represented the flow domain. A no-flux condition at $z = -50$ cm was used for the lower boundary. Initial condition corresponding to a

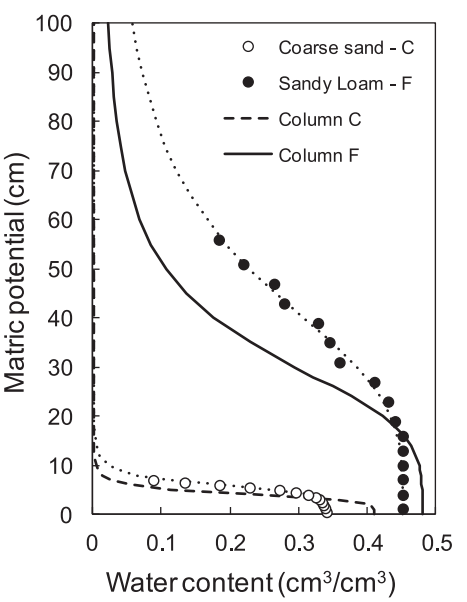

Figure 3. The measured WRC data points and the respective fitted curves using the *van Genuchten* [1980] expression for the coarse sand (C) and the sandy loam (F) (dotted lines), and the estimated WRC (solid and dashed lines) for the soils packed in the columns used in the experiments following correction for differences in bulk density.

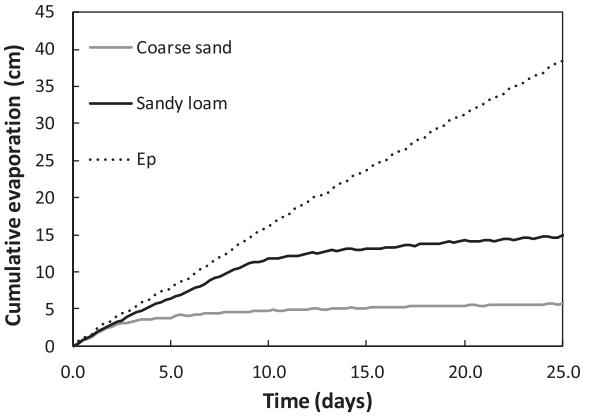

Figure 4. Cumulative evaporation with time for the water-filled column (E_p) and for the homogeneous coarse sand (C) and sandy loam (F) columns.

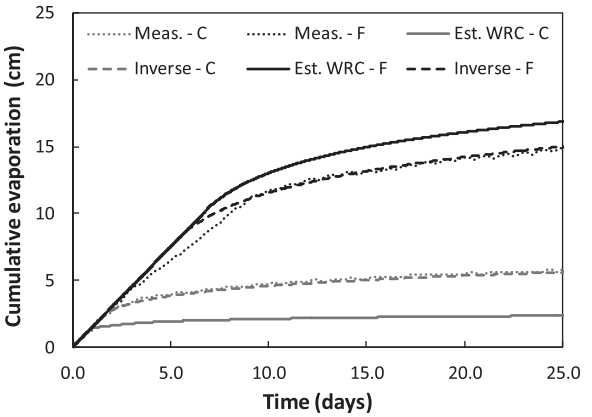

Figure 5. Simulated cumulative evaporation versus time resulting from the numerical solution of Richards equation using Hydrus-1D for the estimated soil hydraulic functions (solid line) and applying the Hydrus inverse procedure (dashed line) by comparison to the measured data (dotted line) for the cases of the homogeneous coarse sand (gray) and sandy loam (black) soils.

saturated soil profile was implemented.

As described in section 3.7, the simulations with the estimated parameters were also used to determine the characteristic length for both soils.

5. Results

5.1. Homogeneous Columns (Capillary-Gravity Regime)

The increase of the cumulative evaporation with time for the water-filled column and for the homogeneous coarse sand and sandy loam ones is depicted in Figure 4. The evaporation rate during *S*1, $e_{S1} \approx 1.2$ cm/d, was lower than the evaporation rate measured on the free water column, $e_0 \approx 1.56$ cm/d. For the conditions in the experiment, e_{S1} is practically constant, thus supporting the assumption made in equation (6). Figure 4 also illustrates well the difference between the coarse and the fine materials with a much longer *S*1 period for the fine material, approximately 2 days for the coarse material versus 9 days for the fine medium, which was expected from the phenomenology simulated in Figures 1a and 1b and described in section 3.

The estimated hydraulic functions corresponding to the soil packed in the columns (*estimated* parameters in Table 1) were used to simulate evaporation from the homogeneous columns by means of the numerical solution of Richards equation provided by Hydrus-1D. The results are shown in Figure 5. The estimated hydraulic functions that were based on measured data (parameters given in Table 1) failed to reproduce the measured cumulative evaporation curve. For the coarse sand, it underestimated the data, while it overestimated it for the sandy loam. Hydrus-1D allows carrying out an inverse procedure aiming to determine

Table 2. Estimate of Characteristic Length and Duration of First Evaporation Stage, *S*1 (Expressed in Terms of Cumulative Evaporation Depth *E*) in the Homogeneous Columns Packed With the Coarse Sand (C) and the Fine Sandy Loam (F)[a]

	Approach A1 [*Lehmann et al.*, 2008]	Approach A2 (This Paper)	Hydrus Simulation	Experiments
Characteristic length L_C (cm) (coarse medium)	2.9	4.2 (4.3)	5.3 (5.4)	
Characteristic length L_F (cm) (fine medium)	33.8	38.1 (39.8)	41.0 (45.0)	
Ratio of characteristic lengths, L_F/L_C	11.6	9.1 (9.2)	7.7 (8.3)	
Evaporation depth E_C (cm) (coarse medium)	0.58	1.0 (1.1)	1.3 (1.4)	3.1
Evaporation depth E_F (cm) (fine medium)	8.1	9.2 (9.8)	9.7 (10.9)	11.1
E_F/E_C	13.9	8.7 (8.9)	7.5 (7.8)	3.6
E_C/L_C	0.20 (equation (19))	0.25 (0.25)	0.25 (0.25)	
E_F/L_F	0.24 (equation (19))	0.24 (0.24)	0.24 (0.24)	

[a]The values for the Hydrus simulations correspond to the *estimated* parameters in Table 1. The potential evaporation rate used in the computations is $e_0 = 1.56$ cm/d (mean evaporation rate from a free water column). Results obtained when using the average evaporation rate measured during *S*1 for the fine material ($e_{S1} \approx 1.2$ cm/d) are indicated in brackets.

the parameters of the soil hydraulic functions leading to the best fit between simulated and measured flow data. This inverse procedure was applied when the measured cumulative evaporation values were used as input. It was possible to reach a good fit between simulated and measured values for the two soil types (Figure 5), but two parameters, n and K_s, had to change significantly comparatively to the estimated values in order to achieve the best fit (Table 1). By adapting the soil hydraulic functions, it is possible to express evaporation in terms of a liquid transport phenomenon without accounting for the essential difference in the physical nature of $S1$ and $S2$ stages. However, it has been shown that this could be valid only as far as the cumulative evaporation is considered and that this approach failed to represent the diurnal dynamics of the evaporation fluxes properly [*Assouline et al*., 2013].

The experimental results are compared in Table 2 with the predictions of the three different approaches with regard to the duration of $S1$ and the thickness of the two-phase zone (i.e., the characteristic length) for the coarse and the fine media, L_C and L_F, respectively. Note that the duration of $S1$ is expressed in terms of the cumulative evaporation depth E at the end of $S1$ (we recall that $E = t_{S1}\, e_{S1}$ and can be approximated by $E \approx t_{S1}\, e_0$). The three approaches, referred to as approaches A1, A2, and Hydrus, are:

A1: the simplified approach proposed in *Lehmann et al*. [2008], which corresponds to equations (1) and (20).

A2: the approach proposed in this paper for both the characteristic length and the evaporation depth, corresponding to equations (26) and (16).

Hydrus: the numerical determination of the characteristic length and the evaporation depth from Hydrus simulations as described in sections 3.7. and 4.2.

Note that the determination of characteristic length is analytical in approaches A1 and A2. The duration estimate of $S1$ is analytical in approach A1 but not in approach A2, which requires the numerical computation of equation (16). The numerical computation of equation (16) using a classical Simpson method [*Press et al*., 1992] is however much simpler than the numerical solution of Richards equation provided in this paper by Hydrus.

Several comments can be made from the results shown in Table 2. First the approach proposed in this paper leads to longer characteristic lengths than the approach proposed by [*Lehmann et al*., 2008]. As can be seen from Table 2, our results are in much better agreement with the results obtained from Hydrus simulations. Our approach, therefore, leads to a seemingly more representative estimate of evaporation depth. Expressed in time unit, our approach leads to duration of $S1$ equal to about 0.67 days for the coarse medium whereas the simpler estimate obtained from the approach in *Lehmann et al*. [2008] leads to a significantly shorter period of 0.37 days. Hydrus leads to a somewhat higher estimate of 0.83 days. However, all approaches underestimate the duration of $S1$ compared to the experimental result ($\approx$2 days). Considering the measured evaporation rate during $S1$ for the sandy loam ($e_{S1} = 1.2$ cm/d) for the potential evaporation rate rather than the value corresponding to the free water experiment ($e_0 = 1.56$ cm/d) improves slightly the estimate (1.13 days for Hydrus and 0.91 days for A2 versus 0.48 days for A1), but still underestimate the duration compared to the experimental data. The difference might be due in part to the evaporation flux distribution at the surface, which is probably not uniform, or to the porosity wall effect (the porosity of a random packing of particles is greater near a wall). *Hidri et al*. [2013] provided an analysis of both effects on drying, which contributes to make the problem two-dimensional and not one dimensional as considered throughout this paper. The contribution of liquid films to the process is also a possible explanation as discussed in more details in section 6. The effect of liquid films would also explain why the Hydrus simulations also underestimate the duration of $S1$. The comparison between the two approaches also indicates that the simple estimate $\frac{1}{2}(\theta_s - \theta_r)$ (equation (19)) slightly overestimates the amounts of water remaining above the drying front at the end of $S1$. For the fine medium, our approach leads again to a greater characteristic length compared to approach A1. Our approach leads to a significantly better comparison with the experimental result and the Hydrus simulation.

It can also be noted that the ratio between the durations of $S1$ (ratio E_F/E_C of evaporation depths at the end of $S1$) and the ratio of characteristic lengths, L_F/L_C, are both closer to the Hydrus simulation in our approach than according to the results of approach A1. This is again mainly due to equation (19) in approach A1, which is based on a somewhat too crude approximation of the water content distribution with depth in the medium at the end of $S1$ in the coarse medium. The ration E_F/E_C is much smaller in the experiment

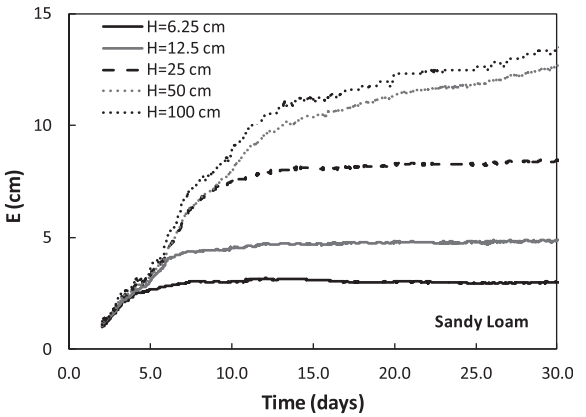

Figure 6. Cumulative evaporation with time for the homogeneous sandy loam columns of various heights H.

(see Table 2), which is due the longer duration of *S*1 with the coarse porous medium compared to theoretical predictions.

5.2. Homogeneous Columns (Capillary Regime)

The validity of equations (27–29) enabling us to estimate the duration of *S*1 in the capillary regime is tested against experimental data. To this end, experiments with the fine soil were performed for columns of various heights. Note that the column diameter is the same as before, namely, 8 cm. The results are depicted in Figure 6. As can be seen, the shorter the column, the shorter *S*1. The capillary-gravity characteristic length L_F is on the order of 34 cm (Table 2). The capillary regime is expected for columns sufficiently shorter than this length. We compare in Figure 7 the prediction given by equation (28) to the experimental results for the columns shorter than L_F, noting that the evaporation rate is on the order of 0.9 cm/d in these experiments. As can be seen, the agreement between the theoretical predictions and the experiments is very good except for the column 25 cm in height. The experimental time is shorter which is consistent with the fact that the column height in this case is not small compared to L_F. Thus, the regime is expected to be a transition regime between the capillary and gravity-capillary regime. In other words, gravity effects are not negligible in the case of the 25 cm column, which results in a shorter *S*1.

5.3. Two-Layer Columns: Fine Over Coarse Case (F/C)

The cumulative evaporation from the soil columns relative to the cumulative evaporation from the water-filled column, E/E_p, is presented as a function of time in Figure 8a and as a function of cumulative evaporation expressed in units of depth in Figure 8b for the fine overlying coarse (*F/C*) cases with different thicknesses H_F ($H_F = 2$, 8, and 12 cm) and for the reference curve characterizing the homogeneous sandy loam case. Note that in all the cases, $L_F > H_F$. The results in Figure 8 illustrate the effect of the thickness of the overlying fine layer on the duration and the cumulative evaporation during *S*1, and on the evaporation rate afterward. The duration of *S*1, and therefore the cumulative evaporation at the end of *S*1, decreases with the increasing thickness of the overlying fine medium. The transition between *S*1 and *S*2 is sharper in the case of the layered systems compared with the homogeneous case. As shown in Figure 8b, the evaporation depths at the end of *S*1 are approximately 4.9, 6.4, and 7.5 cm for the 2, 8, and 12 cm thicknesses, respectively, while it is around 11.1 cm for the homogeneous sandy loam column.

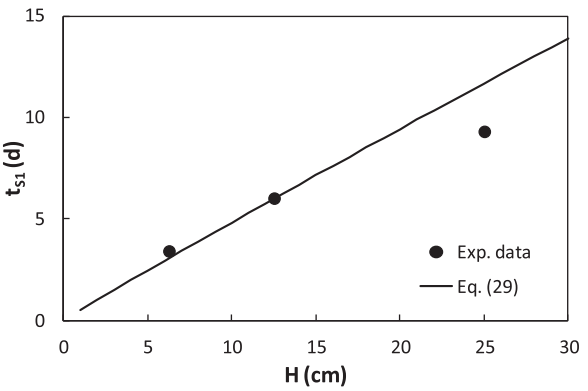

Figure 7. Duration of the *S*1 regime as a function of column height *H* for the sandy loam soil in the capillary regime (equation (28)). The black filled circles are the experimental data.

The estimated hydraulic functions and the ones resulting from the inverse procedure (parameters given in Table 1) were used to simulate evaporation in the *F/C* layered columns (for the 2 and 8 cm sandy loam overlaying layers) by means of the numerical solution of Richards equation in the case of a two-layer system.

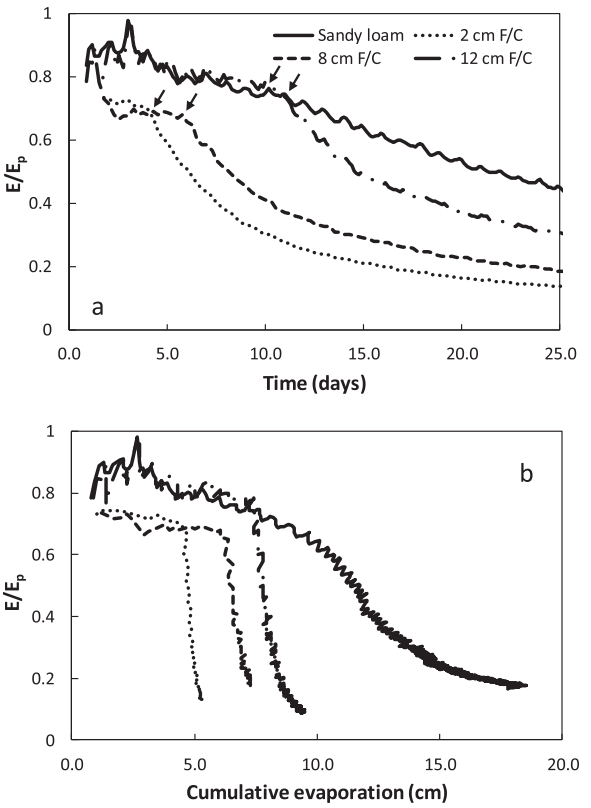

Figure 8. Cumulative evaporation from the soil columns relative to the cumulative evaporation from the water-filled column, E/E_p, as (a) a function of time and as (b) a function of cumulative evaporation expressed in units of depth for the fine overlying coarse (F/C) cases with different thicknesses (2, 8, and 12 cm) and for the reference curve characterizing the homogeneous sandy loam case. The arrows indicate the estimated end of stage 1 evaporation.

The results are shown in Figure 9. None of the two sets of parameters could reproduce the measured data. That means that, in the case of heterogeneous systems, the approach assuming that evaporation could still be expressed in terms of a liquid transport phenomenon during *S*2 is not appropriate. The complex structure of phase distribution with depth illustrated in Figure 1c cannot be captured by simply solving Richards equation while using the hydraulic properties of the porous media that constitute the heterogeneous system.

The comparison between the experimental results and the predictions based on equation (36) is presented in Table 3. To this end we have determined θ_{v-F} from equation (32) using $e_0 = 1.56$ cm/d. This gives the results shown in Figure 10, which indicate that θ_{v-F} is larger than θ_{r-F} by a factor of 3–5, depending on the fine layer thickness. Thus θ_{v-F} is, as expected, small compared to θ_{s-F} but not negligible, and larger than θ_{r-F}. We compared also the results obtained with the computed θ_{v-F} (Figure 10) with the results obtained with the simplification $\theta_{v-F} \approx \theta_{r-F}$ (results in brackets in Table 3).

As can be seen from Table 3, the theoretical prediction of *S1* duration (expressed in terms of cumulative evaporation depth, $E_{F/C}$; equation (36)) is in reasonable agreement with the experimental data if one uses the experimental value for *S*1 duration for the homogeneous coarse column (Table 2). The effect of the fine layer thickness is well captured. The ratio $E_{F/C}/L_{F/C}$ (≈0.5–0.6) is much greater than the value expected for a homogeneous column (≈0.23), based on equation (19) and Table 2. As reported in Table 3, $E_{F/C}/L_{F/C}$ decreases with the increase in the fine layer thickness H_F. According to equation (37), $E_{F/C}/L_{F/C}$ tends toward θ_{s-F} (=0.48) as H_F increases (assuming that θ_{v-F} remains small compared to θ_{s-F}). Naturally, this is valid only when the constraint $L_C \ll H_F \ll L_F$ holds.

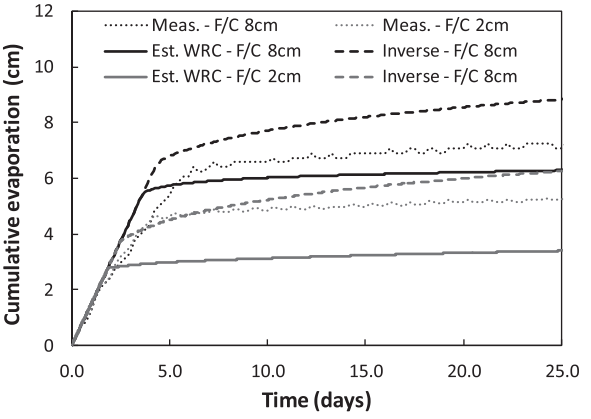

Figure 9. Simulated cumulative evaporation versus time resulting from the numerical solution of Richards equation using Hydrus-1D for the estimated soil hydraulic functions (solid line) and the ones resulting from the application of the inverse procedure (dashed line) by comparison to the measured data (dotted line) for the cases of the F/C-layered system with two upper layer thicknesses, 2 cm (gray) and 8 cm (black).

Table 3. Estimate of Characteristic Length and Estimate *S*1 Duration (Expressed in Cumulative Evaporation Depth) for the Fine Over Coarse System (*F/C*)[a]

H_F (cm)	2	8	12
$E_{F/C}$ (cm) in experiment	4.9	6.4	7.5
$E_{F/C}$ (cm) (equation (36) or equation (38)) with E_c from A2 (=1 cm; Table 2)	1.9 (2.0)	4.5 (4.9)	6.1 (6.8)
$E_{F/C}$ (cm) (equation (36) or equation (38)) with E_C from experiment for homogeneous column (=3.1 cm; Table 2)	4.0 (4.1)	6.5 (6.9)	8.1 (8.9)
$L_{F/C}$ (A2 + equation (34))	6.2	12.2	16.2
$\frac{E_{F/C}}{E_{F/C\exp.}}$	0.79	0.52	0.46
$\frac{E_{F/C}^{L_{F/C}}}{L_{F/C}} \approx \frac{E_C + H_F(\theta_{Fs}-\theta_{Fv})}{L_C+H_F}$ (equation (37) with E_C from experiment)	0.64	0.59	0.54

[a]The potential evaporation rate used in the computations is $e_0 = 1.56$ cm/d.

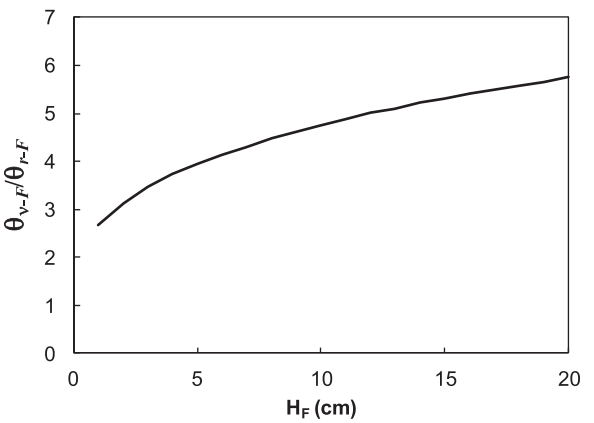

Figure 10. Water content in the fine layer at the end of *S*1 as a function of the overlying fine layer thickness as predicted by equation (29) for the fine/coarse two-layer system (F/C).

5.4. Two-Layer Columns: Coarse Over Fine Case (C/F)

As presented in section 3, dynamics of evaporation in the (*C/F*) case depends on the ratio between the thickness H_C and the characteristic length L_C of the coarse medium. When $L_C \ll H_C$, the problem is straightforward: the presence of the underlying fine porous medium has no influence on the duration of *S*1, which is expected to be controlled by the coarse medium only and $L_{C/F} = L_C$ (equation (40)). This was illustrated in Figure 1e and is shown in Figure 11 where the (*C/F*) configuration with a 12 cm thick coarse layer on top of a column of fine medium behaves exactly like the homogeneous coarse sand column.

The case $L_C > H_C$ is illustrated in Figure 11 where the results obtained for $H_C = 2$ cm are shown. As it can be seen, the results depicted in Figure 11 indicate a shorter stage *S*1 in this case. Application of equations (41) and (42) with $H_C = 2$ cm and the properties of the coarse material leads to $\theta_{v-C} = 0.018$ and $\delta t = 0.52d$ (which corresponds to an evaporation depth $E = 0.81$ cm). This result is in good agreement with the experiment, which indicates a very short stage *S*1 in this case. As it can be seen from Table 2, the evaporation depth at the end of *S*1 is lower here than for the homogeneous coarse material, which is in agreement with the experimental results reported in Figure 11.

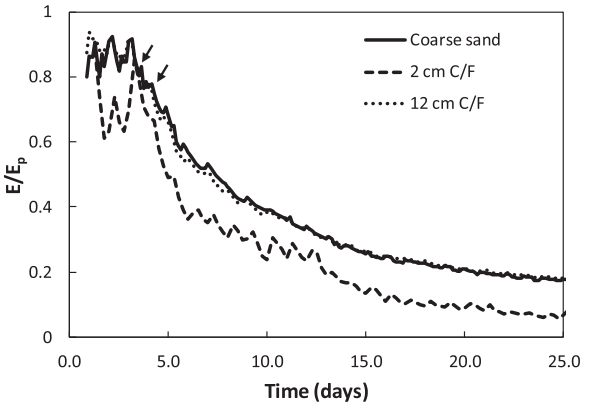

Figure 11. Relative evaporation, E/E_p, versus time for 2 and 12 cm thick layer of coarse sand overlying sandy loam (C/F) and for the homogeneous column of coarse sand. The arrows indicate the estimated end of stage 1 evaporation.

6. Discussion

6.1. Effect of Overlaying Layer

The effect of the properties of the overlying layer in our experiments is summarized in Figures 8 and 11, where the relative evaporation curves from several (*C/F*) and (*F/C*) configurations can be compared with the reference curves of the homogeneous columns of sandy loam and coarse sand. The (*C/F*) configuration behaves exactly like the

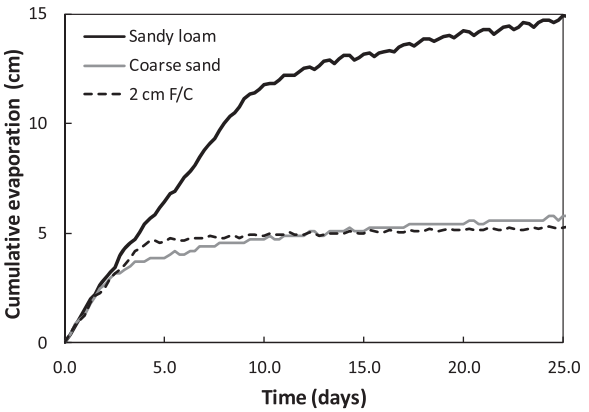

Figure 12. Cumulative evaporation versus time for 2 cm thick layer of sandy loam overlying coarse sand (2 cm F/C) column, and reference evaporation curves for the homogeneous columns of sandy loam and coarse sand.

homogeneous coarse sand column since the thickness of the overlying layer exceeds its own characteristic length, as it is illustrated in Figure 1e. In such case, the properties of the top layer determine the behavior of the overall column. However, coarse layer thicknesses smaller than the characteristic length of the medium reduce water losses from evaporation by comparison to a homogeneous medium. Similarly, the (*F/C*) configuration reduces the evaporation losses compared to the homogeneous sandy loam column because its thickness is smaller than its characteristic length. On the other hand, it increases the evaporation losses compared to the homogeneous coarse sand column because of its longer combined characteristic length, thus inducing a more complex structure of phase distribution with depth (Figure 1c).

As presented in section 1, the (*F/C*) configuration increases evaporation losses [*Shokri et al*., 2010], does not affect it much [*Willis*, 1960], or, in some cases like during soil surface sealing, could reduce it [*Bresler and Kemper*, 1970; *Assouline and Mualem*, 2003]. This can be qualitatively understood from the consideration of the various length scales involved in the problem. We have two geometrical length scales: the thicknesses H_F and H_C of the fine and coarse layers and two characteristic length scales L_C and L_F characterizing the extent of two-phase zone within homogeneous samples at the end of *S*1. As shown in our experiments, the (*F/C*) configuration increases evaporation losses as also reported in *Shokri et al*. [2010] when $L_C < H_F < H_C < L_F$. To obtain a reduction in the evaporation losses as reported in *Bresler and Kemper* [1970] and *Assouline and Mualem* [2003], an obvious possibility is $L_F < H_F < L_C < H_C$. This is of course not possible if the distribution of the liquid in both media coarse and fine process is dominated by capillary and gravity effects only. This is however possible if viscous effects are sufficient to control the extent of two-phase zone in the fine medium [*Shaw*, 1987; *Lehmann et al*., 2008]. This corresponds to the viscous-capillary regime mentioned in section 3.1. Thus, a layer of sufficiently fine medium on top of a coarse porous medium can in this case reduce the evaporation loss compared to the case of the homogeneous coarse porous medium. Then, if the viscous-capillary characteristic length of the fine medium $L_{vis\text{-}F}$ is on the same order as the gravity-capillary characteristic length L_C of that medium, and both are lower than the fine layer thickness H_F, i.e., $L_{vis\text{-}F} \approx L_C < H_F < H$, then the presence of the fine layer will not modify the duration of *S*1 compared to the case of the homogeneous coarse porous medium.

The discussion presented above applies when one is interested in the duration of *S*1, which is the phase of high evaporation. As illustrated in Figure 12, which shown the effect of a relatively thin, 2 cm thick, overlying fine layer for our conditions, the situation can be subtler if one looks at the evaporation losses over a longer period. Compared to the reference cumulative evaporation curve of the coarse sand, the 2 cm (*F/C*) configuration increases the evaporation losses during *S*1 but then the evaporation rate decreases drastically and after 15 days, less water evaporated from this column compared to the homogeneous coarse one. It is interesting to see that in this figure, all the three apparently contradictory trends listed above are valid, depending on the duration of the process. The slower drying at long times with the (*F/C*) system is explained by the fact that the fine layer, once dry, eventually adds an additional vapor diffusive resistance to the vapor transfer between the coarse medium and the external air.

6.2. Characteristic Length and Film Flow

Although the approach proposed in the present paper for determining the characteristic length and the duration of *S*1 leads to a reasonably good result with regards to the fine medium, the prediction is poor for the coarse medium (the duration of *S*1 is underpredicted by a factor of 3 as reported in Table 2). As discussed in several previous studies [e.g., *Yiotis et al*., 2012, and references therein], the hydraulic connectivity

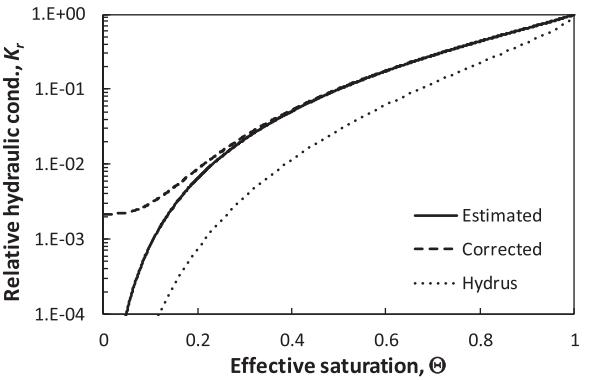

Figure 13. The unsaturated hydraulic conductivity functions of the coarse sand. The solid line is the estimated unsaturated hydraulic conductivity of the homogeneous column (Table 1 and equation (23)); the dashed line represents the modified unsaturated hydraulic conductivity to account for film effects (see section 6.1.); the dotted line is the function resulting from the application of Hydrus using the inverse procedure (Table 1 and equation (23)).

to the surface can be maintained via liquid films, even when bulk-phase connectivity ends. The result is a much longer $S1$ than predicted from the consideration of the bulk phase connectivity. A simple procedure to mimic the effect of liquid films is to increase the hydraulic conductivity when θ approaches θ_r. As an example, we have used a modified hydraulic conductivity of the form $K_{\mathrm{mod}}(\Theta)=K(\Theta)+\eta K_s$, where η is a small parameter. The factor ηK_s is supposed to represent the liquid film hydraulic conductivity. With $\eta = 2.15 \times 10^{-3}$, one obtains the variation of hydraulic conductivity depicted in Figure 13, which is different from the original hydraulic conductivity (as given by the Mualem model; see equation (23)) only in the region of very low water contents. Other methods could also be applied that would lead to similar type of corrections [*Assouline and Or*, 2013]. With this modified conductivity, our approach leads to $L_C \approx 9.3$ cm and $E_C = 3.1$ cm for the coarse medium in excellent agreement with the experimental data (Table 2). It is interesting to note that the $K_r(\Theta)$ function resulting from applying the inverse procedure to fit the numerical solution of Richards equation to the data for the homogenous coarse sand column (Table 1) differs significantly from the estimated one (dotted line in Figure 13). This emphasizes the importance of the hydraulic gradient at the vicinity of the drying soil surface when applying the conventional continuum approach to evaluate evaporation fluxes. To set the modification of the hydraulic conductivity on a sound basis, it would be interesting to derive the hydraulic conductivity as well as the capillary pressure from corner flow theory. This interesting problem is beyond the scope of the present effort and therefore left for a future work.

Regarding the fine medium, it should be noted that the theoretical prediction also underestimates the duration of $S1$, but much less than for the coarse medium (the predicted evaporation depth E_F is about only 12% lower than the experimental value in Table 2). This can be regarded as an indication that the liquid film effect is still present. One question is thus why the film effects would be quite significant in the coarse sand and less effective in the fine soil since the agreement between our theoretical prediction and the experiment is much better with the fine soil (Table 2). From the data, one can estimate the maximum extent of film regions assuming that the amount of water in the films is negligible compared to the amount of water contained in a liquid water saturated region of same extent. This leads to express the extent ζ of films region as

$$\zeta = \frac{\left(E_{\mathrm{exp}} - E_{comp}\right)}{\theta_s} \tag{44}$$

where E_{exp} and E_{comp} are the experimental and computed evaporation depth, respectively. Using equation (44) leads to $\zeta_C = 5$ cm and $\zeta_F = 2.6$ cm, meaning that the liquid film extents greater than the theoretical characteristic length for the coarse medium and is equal to about 7% of the characteristic length for the fine medium. Thus the error is in fact less with the fine soil because (i) the characteristic length of the fine medium is much greater; (ii) the extent of film regions is twice as short. As a result the relative error on the evaporation depth E is much less for the fine soil. As discussed in *Chauvet et al.* [2009] or *Yiotis et al.* [2012], the extent of liquid films depends on the competition between capillary, gravity, and viscous forces. Both gravity and viscous effects tend to limit the extent of liquid films. The mean particle diameters are on the order of 1 mm in the coarse sand and 0.1 mm in the fine soil. Viscous effects are therefore relatively more

important in the fine soil since the particle size is smaller whereas gravity effects can be expected to be relatively more important in the coarse material owing to the relatively big size of the particles. Thus the relative importance of viscous and gravity effects on the liquid films is different in both media and this should explain the difference in film extent between the two media estimated from equation (44).

7. Conclusions

Pore network simulations were used to illustrate the structure of phase distribution during evaporation for the various systems considered. These simulated results and the experimental data confirm that adding a narrow layer of porous medium (other soil, mulch, etc.) having different properties from the underlying main soil is a simple means of controlling evaporation losses. Adding a coarser material reduces the evaporation losses because of the preferential invasion by the gas phase of the larger pores of the coarse material. Adding a finer material can either increase or reduce the evaporation losses depending on the characteristic length of the fine material. For example, a sufficiently fine material will reduce the evaporation losses because of the influence of viscous effects on the characteristic length of the fine material. If the fine material is too coarse for generating significant pressure drops due to viscous effects, then the expected effect is an increase of *S*1 duration. As shown in this paper, the duration of *S*1 then increases with the thickness of fine material in this case. The concept of characteristic length is therefore useful to delineate the various situations.

The method proposed by *Lehmann et al*. [2008] can be used to evaluate the characteristic length and the duration of *S*1. In this paper, we have proposed an alternative way of determining the characteristic length for the regime where the two-phase zone extent is mainly controlled by the capillary and gravity effects. In addition to the retention curve, our method necessitates the knowledge of the unsaturated hydraulic conductivity. Our method leads to longer characteristic lengths compared to the method of *Lehmann et al*. [2008], in much better agreement with Hydrus simulations. It leads to results closer to the experimental data, at least for the experiments discussed in this paper. More comparisons are certainly desirable to confirm this trend. We have also proposed a method to evaluate the duration of stage *S*1 in the case of the (*F/C*) system when the capillary-gravity characteristic length of the fine material is much greater that the thickness of the top fine layer. A good agreement was found with experimental data as regards the duration of *S*1.

However, the observed discrepancies between the theoretical predictions and the experimental results on the duration of *S*1 for the homogeneous columns suggest a significant effect of liquid films in accordance with previous works. As a result, the predictions based of the characteristic length as defined in this paper or on the Hydrus simulations should be regarded only as conservative estimates underestimating the extent of the constant-rate period. This is because the upper layer of the medium continues being in the *S*1 regime owing to effect of liquid films, even after bulk connectivity ends.

Acknowledgments

Financial support from the Israeli French High Council for Scientific and Technological Research (Project ISRAEL 10 F 8/EAU) is gratefully acknowledged. Contribution of the Agricultural Research Organization, Institute of Soil, Water and Environmental Sciences, Bet Dagan, Israel is also acknowledged (606/13). The data in this study are available upon request.

References

Assouline, S. (2004), Rainfall-induced soil surface sealing: A critical review of observations, conceptual models and solutions, *Vadose Zone J.*, *3*, 570–591.

Assouline, S. (2006a), Modeling the relationship between soil bulk density and the hydraulic conductivity function, *Vadose Zone J.*, *5*, 697–705, doi:10.2136/vzj2005.0084.

Assouline, S. (2006b), Modeling the relationship between soil bulk density and the hydraulic conductivity function, *Vadose Zone J.*, *5*, 697–705.

Assouline, S., and Y. Mualem (1997), Modeling the dynamics of seal formation and its effect on infiltration as related to soil and rainfall characteristics, *Water Resour. Res.*, *33*(7), 1527–1536.

Assouline, S., and Y. Mualem (2003), Effect of rainfall induced soil seals on the soil water regime: Drying interval and subsequent wetting, *Transp. Porous Media*, *53*, 75–94.

Assouline, S., and D. Or (2013), Conceptual and parametric representation of soil hydraulic properties: A review, *Vadose Zone J.*, *12*, 1–20, doi:10.2136/vzj2013.07.0121.

Assouline, S., J. Selker, and J.-Y. Parlange (2007), A simple accurate method to predict time of ponding under variable intensity rainfall, *Water Resour. Res.*, *43*, W03426, doi:10.1029/2006WR005138.

Assouline, S., S. W. Tyler, J. S. Selker, I. Lunati, C. W. Higgins, and M. B. Parlange (2013), Evaporation from a shallow water table: Diurnal dynamics of water and heat regime at the surface of drying sand, *Water Resour. Res.*, *49*, 1–13, doi:10.1002/wrcr.20293.

Bresler, E., and W. D. Kemper (1970), Soil water evaporation as affected by wetting methods and crust formation, *Soil Sci. Soc. Am. Proc.*, *34*, 3–8.

Bristow, K. L., and R. Horton (1996), Modeling the impact of partial surface mulch on soil heat and water flow, *Theor. Appl. Climatol.*, *54*, 85–98.

Brooks, R. H., and A. T. Corey (1964), Hydraulic properties of porous media, *Hydrol. Pap. 3*, p. 27, Colo. State Univ., Fort Collins.
Brutsaert, W. (2005), *Hydrology—An Introduction*, 618 pp., Cambridge Univ. Press, N. Y.
Chapuis, O., and M. Prat (2007), Influence of wettability conditions on slow evaporation in two-dimensional porous media, *Phys. Rev. E*, *75*, 046311.
Chauvet, F., P. Duru, S. Geoffroy, and M. Prat (2009), Three periods of drying of a single square capillary tube, *Phys. Rev. Lett.*, *103*, 124502.
Chraibi, H., M. Prat, and O. Chapuis (2009), Influence of contact angle on slow evaporation in two dimensional porous media, *Phys. Rev. E*, *79*, 026313.
Coussot, P. (2000), Scaling approach to the convective drying of a porous medium, *Eur. Phys. J. B*, *15*, 557–566.
Diaz, F., C. C. Jimenez, and M. Tejedor (2005), Influence of the thickness and grain size of tephra mulch on soil water evaporation, *Agric. Water Manage.*, *74*(1), 47–55, doi:10.1016/j.agwat.2004.10.011.
Haghighi, E., E. Shahraeeni, P. Lehmann, and D. Or (2013), Evaporation rates across a convective air boundary layer are dominated by diffusion, *Water Resour. Res.*, *49*, 1602–1610, doi:10.1002/wrcr.20166.
Hidri, F., N. Sghaier, H. Eloukabi, M. Prat, and S. B. Nasrallah (2013), Porous medium coffee ring effect and other factors affecting the first crystallization time of sodium chloride at the surface of a drying porous medium, *Phys. Fluids*, *25*, 127101.
Holmes, J. W., E. L. Greacen, and C. G. Gurr (1960), The evaporation of water from bare soils with different tilths, in *7th International Congress of Soil Science*, pp. 188–194, Soil Science Society of America, Madison, Wis.
Huinink, H. P., L. Pel, M. A. J. Michels, and M. Prat (2002), Drying processes in the presence of temperature gradients. Pore-scale modeling, *Eur. Phys. J. E*, *9*, 487–498, doi:10.1140/epje/i2002-10106-1.
Laurindo, J. B., and M. Prat (1996), Numerical and experimental network study of evaporation in capillary porous media. Phase distributions, *Chem. Eng. Sci.*, *51*(23), 5171–5185.
Laurindo, J. B., and M. Prat (1998), Numerical and experimental network study of evaporation in capillary porous media: Drying rates, *Chem. Eng. Sci.*, *53*, 2257–2269, doi:10.1016/S0009-2509(97)00348-5.
Le Bray, Y., and M. Prat (1999), Three dimensional pore network simulation of drying in capillary porous media, *Int. J. Heat Mass Transfer*, *42*, 4207–4224.
Lehmann, P., and D. Or (2009), Evaporation and capillary coupling across vertical textural contrasts in porous media, *Phys. Rev. E*, *80*, 046318, doi:10.1103/PhysRevE.80.046318.
Lehmann, P., S. Assouline, and D. Or (2008), Characteristic lengths affecting evaporative drying of porous media, *Phys. Rev. E*, *77*, 056309, doi:10.1103/PhysRevE.77.056309.
Mellouli, H. J., B. van Wesemael, J. Poesen, and R. Hartmann (2000), Evaporation losses from bare soils as influenced by cultivation techniques in semi-arid regions, *Agric. Water Manage.*, *42*, 355–369, doi:10.1016/S0378–3774(99)00040-2.
Milly, P. C. D. (1984), A simulation analysis of thermal effects on evaporation from soils, *Water Resour. Res.*, *20*(8), 1087–1098.
Modaihsh, A. S., R. Horton, and D. Kirkham (1985), Soil water evaporation suppression by mulches, *Soil Sci.*, *139*(4), 357–361, doi:10.1097/00010694–198504000-00010.
Moldrup, P., T. Olesen, J. Gamst, P. Schjønning, T. Yamaguchi, and D. E. Rolston (2000), Predicting the gas diffusion coefficient in repacked soil: Water-induced linear reduction model, *Soil Sci. Soc. Am. J.*, *64*, 1588–1594.
Moroizumi, T., and H. Horino (2002), The effects of tillage on soil temperature and soil water, *Soil Sci.*, *167*, 548–559.
Mualem, Y. (1976), A new model for predicting the hydraulic conductivity of unsaturated porous media, *Water Resour. Res.*, *12*(3), 513–522.
Or, D., P. Lehmann, E. Shahraeeni, and N. Shokri (2013), Advances in soil evaporation—A review, *Vadose Zone J.*, *12*(4), 6, doi:10.2136/vzj2012.0163.
Philip, J. R. (1957), Evaporation and moisture and heat fields in the soil, *J. Meteorol.*, *14*, 354–366.
Pillai, K. M., M. Prat, and M. Marcoux (2009), A study on slow evaporation of liquids in a dual-porosity porous medium using square network model, *Int. J. Heat Mass Transfer*, *52*, 1643–1656, doi:10.1016/j.ijheatmasstransfer.2008.10.007.
Plourde, F., and M. Prat (2003), Pore network simulations of drying of capillary media. Influence of thermal gradients, *Int. J. Heat Mass Transfer*, *46*, 1293–1307.
Prat, M. (1993), Percolation model of drying under isothermal conditions in porous media, *Int. J. Multiphase Flow*, *19*(4), 691–704.
Prat, M. (2002), Recent advances in pore-scale models for drying of porous media, *Chem. Eng. J.*, *86*(1–2), 153–164.
Prat, M. (2007), On the influence of pore shape, contact angle and film flows on drying of capillary porous media, *Int. J. Heat Mass Transfer*, *50*, 1455–1468.
Prat, M. (2011), Pore network models of drying, contact angle and films flows, *Chem. Eng. Technol.*, *34*(7), 1029–1038.
Prat, M., and F. Bouleux (1999), Drying of capillary porous media with stabilized front in two dimensions, *Phys. Rev. E*, *60*, 5647–5656.
Prat, M., S. Veran-Tissoires, N. Vorhauer, T. Metzger, and E. Tsotsas (2012), Fractal phase distribution and drying: impact on two-phase scaling and drying time scale dependence, *Drying Technol. J.*, *30*(11-12), 1129–1135.
Press, W. H., S. A. Teukolsky, W. T. Vetterling, and B. P. Flannery (1992), *Numerical Recipes in Fortran 77. The Art of Scientific Computing*, 2nd ed., Cambridge Univ. Press, New York.
Saito, H., J. Simunek, and B. P. Mohanty (2006), Numerical analysis of coupled water, vapor, and heat transport in the vadose zone, *Vadose Zone J.*, *5*, 784–800.
Sakai, M., N. Toride, and J. Simunek (2009), Water and vapor movement with condensation and evaporation in a sandy column, *Soil Sci. Soc. Am. J.*, *73*, 707–717, doi:10.2136/sssaj2008.0094.
Salvucci, G. D. (1997), Soil and moisture independent estimation of stage-2 evaporation from potential evaporation and albedo or surface temperature, *Water Resour. Res.*, *33*(1), 111–122.
Saravanapavan, T., and G. D. Salvucci (2000), Analysis of rate-limiting processes in soil evaporation with implications for soil resistance models, *Adv. Water Resour.*, *23*, 493–502, doi:10.1016/S0309–1708(99)00045-7.
Scherer, G. W. (1990), Theory of drying, *J. Am. Ceram. Soc. 73*, *3-14*.
Shahraeeni, E., P. Lehmann, and D. Or (2012), Coupling of evaporative fluxes from drying porous surfaces with air boundary layer: Characteristics of evaporation from discrete pores, *Water Resour. Res.*, *48*, W09525, doi:10.1029/2012WR011857.
Shaw, T. M. (1987), Drying as an immiscible displacement process with fluid counterflow, *Phys. Rev. Lett.*, *59*(15), 1671–1674.
Shimojima, E., A. A. Curtis, and J. V. Turner (1990), The mechanisms of evaporation from sand columns with restricted and unrestricted water tables using Deuterium under turbulent air flow conditions, *J. Hydrol.*, *117*, 15–54.
Shokri, N., and G. D. Salvucci (2011), Evaporation from porous media in the presence of a water table, *Vadose Zone J.*, *10*, 1309–1318, doi:10.2136/vzj2011.0027.
Shokri, N., P. Lehmann, and D. Or (2009), Critical evaluation of enhancement factors for vapor transport through unsaturated porous media, *Water Resour. Res.*, *45*, W10433, doi:10.1029/2009WR007769.

Shokri, N., P. Lehmann, and D. Or (2010), Evaporation from layered porous media, *J. Geophys. Res.*, *45*, W10433, doi:10.1029/2009WR007769.

Simunek, J., M. Th. van Genuchten, and M. Sejna (2005), *The HYDRUS-1D Software Package for Simulating the Movement of Water, Heat, and Multiple Solutes in Variably Saturated Media, Version 3.0, HYDRUS Software Ser. 1*, p. 270, Dep. of Environ. Sci., Univ. of Calif. Riverside, Riverside.

Unger, P. W. (1971), Soil profile gravel layers: I. Effect on water storage, distribution and evaporation, *Soil Sci. Soc. Am. Proc.*, *35*, 631–634.

van Brakel, J. (1980), Mass transfer in convective drying, *Adv. Drying*, *1*, 212–267.

van Genuchten, M. T. (1980), A closed-form equation for predicting the hydraulic conductivity of unsaturated soils, *Soil Sci. Soc. Am. J.*, *44*, 892–898.

Veran-Tissoires, S., M. Marcoux, and M. Prat (2012), Discrete salt crystallization at the surface of a porous medium, *Phys. Rev. Lett.*, *108*, 054502.

Whitaker, S. (1998), Coupled transport in multiphase systems. A theory of drying, *Adv. Heat Transfer*, *31*, 1–104.

Wilkinson, D., and J. F. Willemsen (1983), Invasion percolation: A new form of percolation theory, *J. Phys. A*, *16*, 3365–3376.

Willis, W. O. (1960), Evaporation from layered soils in the presence of a water table, Soil Sci. Soc. *Am. Proc.*, *24*, 239–242.

Yamanaka, T., and T. Yonetani (1999), Dynamics of the evaporation zone in dry sandy soils, *J. Hydrol.*, *217*, 135–148, doi:10.1016/S0022-1694(99)00021-9.

Yamanaka, T., M. Inoue, and I. Kaihotsu (2004), Effects of gravel mulch on water vapor transfer above and below the soil surface, *Agric. Water Manage.*, *67*, 145–155 doi:10.1016/j.agwat.2004.01.002.

Yiotis, A. G., A. G. Boudouvis, A. K. Stubos, I. N. Tsimpanogiannis, and Y. C. Yortsos (2003), The effect of liquid films on the isothermal drying of porous media, *Phys. Rev. E*, *68*(3), 037303.

Yiotis, A. G., I. N. Tsimpanogiannis, A. K. Stubos, and Y. C. Yortsos (2006), Pore-network study of the characteristic periods in the drying of porous media, *J. Colloid Interface Sci.*, *297*, 738–748, doi:10.1016/j.jcis.2005.11.043.

Yiotis, A. G., D. Salin, E. S. Tajerand, and Y. C. Yortsos (2012), Drying in porous media with gravity-stabilized fronts: Experimental results, *Phys. Rev. E*, *86*, 026310.